Supplementary Information

Controlled Bioorthogonal Catalyst Self-Assembly and Activity Using Rationally Designed Polymer Scaffolds

Rui Huang[†], Cristina-Maria Hirschbiegel[†], David C. Luther[†], Cheng-Hsuan Li[†], Ahmed Nabawy[†], Jungmi Park[†], Alexander Ribbe[††], Yisheng Xu[§, *] and Vincent M. Rotello[†,*]

† Department of Chemistry, University of Massachusetts Amherst, 710 North Pleasant Street, Amherst, Massachusetts 01003, United States

†† Department of Polymer Science and Engineering, University of Massachusetts Amherst, 120 Governors Dr, Amherst, MA 01003, United States

§ State Key Laboratory of Chemical Engineering, East China University of Science and Technology, Shanghai, 200237 P. R. China

Table of Contents

1. Materials

All chemicals and solvents for syntheses were purchased from Fisher Scientific and Sigma-Aldrich, and used without further purification unless otherwise stated. The chemicals were used as received. All reagents and solvents were purchased from Fisher Scientific and used as received. The yields of the compounds reported here refer to the yields of spectroscopically pure compounds after purification. ^{1}H NMR spectra were recorded at 400 MHz on a Bruker ADVANCE 400 machine.

2. Oxanorbornene Polymer Synthesis

Synthesis of monomers

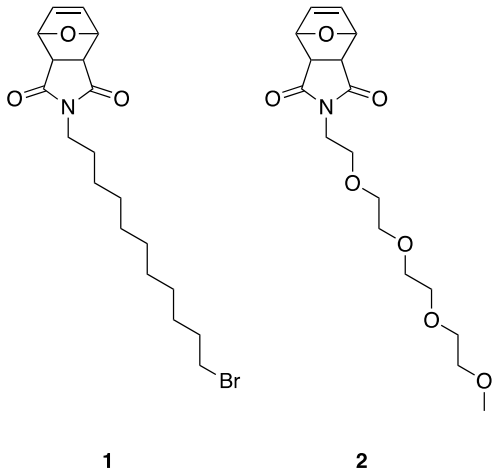

Supplementary Figure S1: Structure of monomers ONI-C11Br (**1**) and ONI-TegOMe (**2**).

ONI-C11Br (**1**) and ONI-TegOMe (**2**) were synthesized according to the procedures previously reported in the literature.[1,2]

Synthesis of PONI-C_{11}-Br-TEG-OMe (3)

To a 10 mL air-free flask equipped with a stir-bar was added **1** (200 mg, 0.51 mmol, 9 eq), **2** (20 mg, 0.051 mmol, 1 eq) and 4 mL of dichloromethane (DCM). In a separate 10 mL air-free flask was added Grubbs 3rd generation catalyst (5.59 mg, 0.0603 mmol) and 1mL of DCM. The flasks were sealed with septa and then both flasks were freeze-pump-thawed three times. Subsequently, the catalyst solution was transferred to the flask containing the monomers and allowed to react for 20 min. Ethyl vinyl ether (300 µL) was added and allowed to stir for 15 min. The reaction mixture was then diluted to two times the volume and precipitated into a heavily stirred solution of hexane (500 mL) to yield Polymer **3**. MW = 37300, PDI = 1.15, as determined by THF GPC using a polystyrene calibration curve. ^{1}H NMR (400MHz, $CDCl_3$, δ) 6.08 (br s, 1H, =C*H*-CH-O of the backbone), 5.78 (br m, 1H, O-CH-C*H*= of the backbone), 5.03 (br m, 1H, =CH-C*H*-O of the backbone), 4.46 (br s, 2H, =CH-C*H*-O of the backbone), 3.75-3.25 (br

m, 25H, overlapping of C(O)-N-CH_2 and CH_2-CH_2-Br of **1**, N-CH_2-CH_2-O and O-CH_2-CH_2-O of **2**), 1.85 (quin, 2H, CH_2-CH_2-Br of **1**), 1.55 (br quin, 2H, -CH_2-CH_2-CH_2-Br and CH_2-CH_2-N of **1**), 1.41 (quin, 2H, CH_2-CH_2- CH_2- CH_2-Br of **1**), 1.27 (m, 12 H, CH_2-CH_2-CH_2 of **1**). Synthesis scheme in Supporting Information **(Figure S2)**.

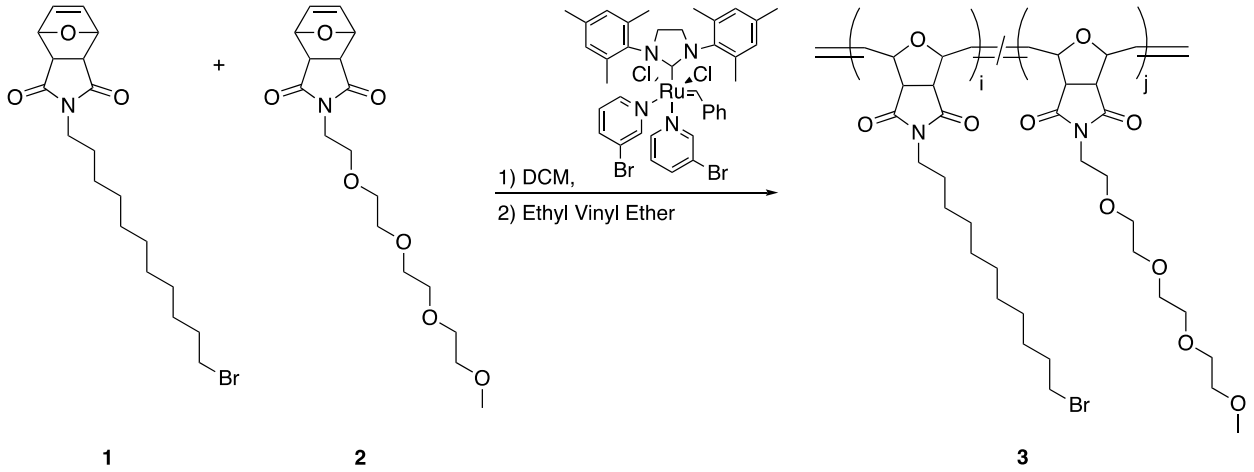

Supplementary Figure S2: Synthesis scheme of PONI-C_{11}-Br-TEG-OMe.

Synthesis of PONI-C_{11}-TMA-TEG-OMe (4)

PONI-C11TMA-TegOMe (**3**, 200 mg) was added to a 20 mL vial with a stir bar. Subsequently, excess of trimethylamine (0.55 mL of 1M trimethylamine in THF) was added to the vial. The reaction was run 2 days at 50 °C. Afterwards, the solvent was removed, and the product was dissolved in Milli-Q water. The polymer solution was transferred to 10,000 MWCO dialysis membrane and allow to stir for 3 days with water changed periodically. After that, the polymer solution was filtered with PES syringe filters and freeze-dried to yield 4. 1H NMR (400MHz, D2O, δ) 6.08 (br s, 1H, =CH-CH-O of the backbone), 5.9 (br m, 1H, O-CH-CH= of the backbone), 4.92 (br m, 1H, =CH-CH-O of the backbone), 4.52 (br s, 2H, =CH-CH-O of the backbone), 3.75-3.11 (br m, 34H, overlapping of C(O)-N-CH2 and CH2-CH2-N-(CH3)3, CH2-CH2-N-(CH3)3),N-CH2-CH2-O and O-CH2-CH2-O of 2), 1.81 (quin, 2H, CH2-CH2-N-(CH3)3), 1.54 (br quin, 2H, CH2-CH2-N of 1), 1.38 and 1.3 (br s, 12 H, CH2-CH2-CH2 of 1). Synthesis scheme in Supporting Information **(Figure S3)**.

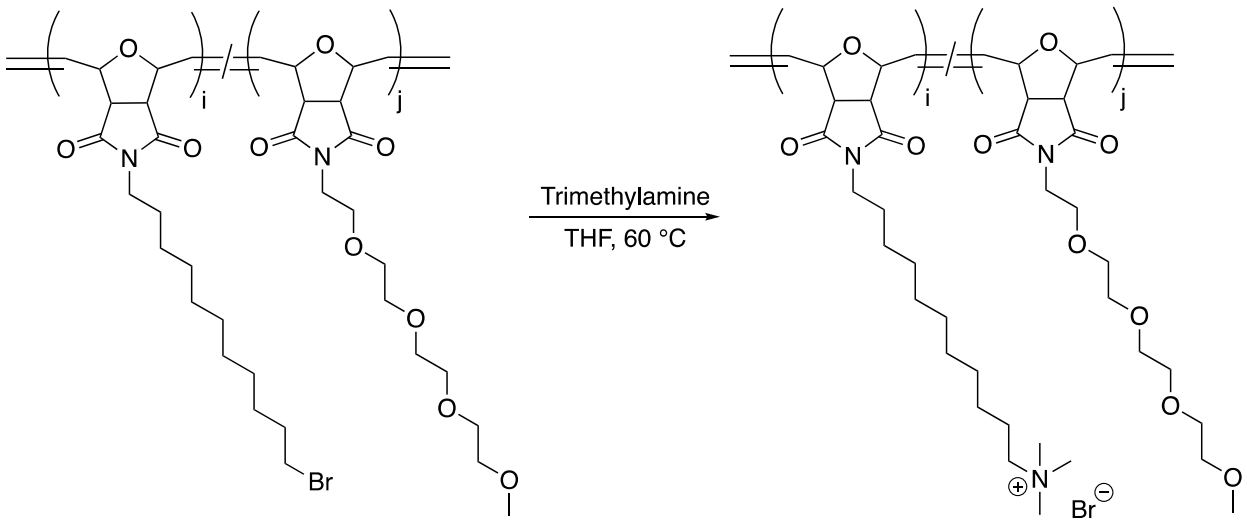

3 4

Supplementary Figure S3: Synthesis scheme of PONI-C_{11}-TMA-TEG-Ome.

3. Comparison between the Classic Precipitation Procedure and FNP Approach

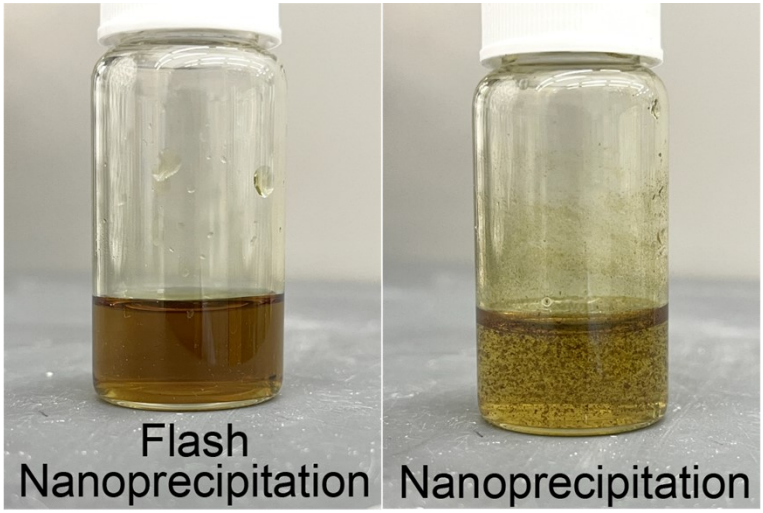

Supplementary Figure S4: The nanocatalyst prepared through flash nanoprecipitation (FNP) exhibited remarkable stability without any observed precipitation. In contrast, the nanocatalyst fabricated by classic mixing (nanoprecipitation) showed significant precipitation immediately after mixing. After mixing, the precipitate is filtered. Both nanocatalysts utilized the PONI-30%TEG-OMe polymer with a polymer-to-catalyst ratio of 1:10 (**TMA_70_TEG_30_1:10**).

4. Catalyst encapsulation into polymer scaffold

Nanocatalysts were generated via FNP using a confined impinging jet (CIJ) mixer composed of two separate streams. The typical procedure for nanocatalyst preparation is as follows. Each mixer inlet was connected to a 1 mL all-plastic syringe. For mixing, 0.6 mL of the FeTPP catalyst solution in THF was loaded in one syringe, while 0.6 mL of the polymer solution in water was loaded into the other. The two streams were then manually impinged into the CIJ mixer rapidly and simultaneously. The outlet of the CIJ mixer was connected to a quench bath containing 5 mL of water. Samples were further centrifuged with a centrifuge filter (10 kDa) for five times to remove any unbound catalysts and the remaining organic solvent and subsequently filtered through a 0.45 μm syringe filter. The amount of encapsulated catalyst was quantified *via* UV/Vis spectroscopy using a standard calibration curve **(Figure S5** and **S9),** and the nanoparticle size was determined *via* dynamic light scattering, transmission electron microscopy, and elemental mapping **(Figure S8)**.

5. Quantification of FeTPP loaded in nanocatalyst

The quantification of Fe catalysts per particle was carried out by first drying 100 μL nanocatalyst (0.05 mg/mL, 1.5 μM) under flowing nitrogen. Then the sample was redissolved in 3mL of THF and filtered through a PTFE syringe filter. The amount of loaded [Fe(TPP)]Cl was then quantified by UV-Vis. Standard [Fe(TPP)]Cl solutions were prepared for constructing the calibration curve.

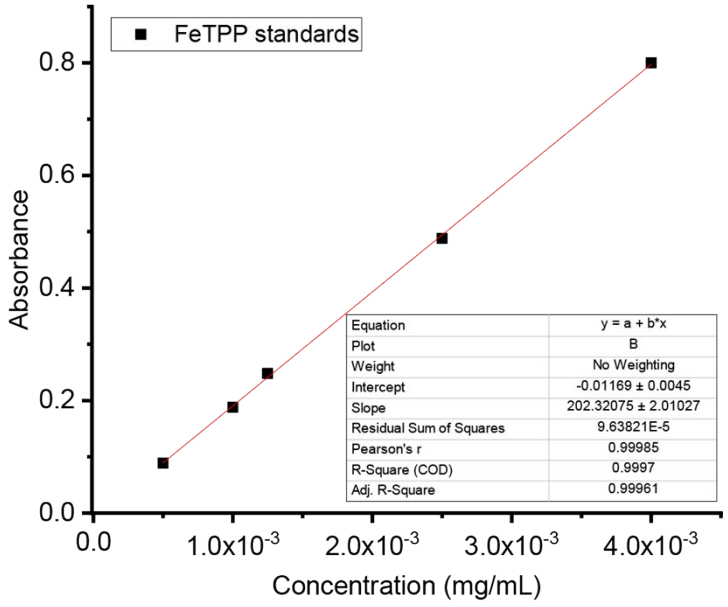

Supplementary Figure S5: Standard calibration curve of FeTPP solution.

6. Characterization of nanozymes

6.1. UV/Vis spectroscopy

The polyzymes TMA_70_TEG_30_1:1 and TMA_100_Teg_0_1:1 were characterized by UV/Vis at a concentration of 0.04 mg/mL of each respective polyzyme (**Figure S6**). Both polyzyme species show absorbance spectra that match the UV/Vis spectrum of FeTPP.[3]

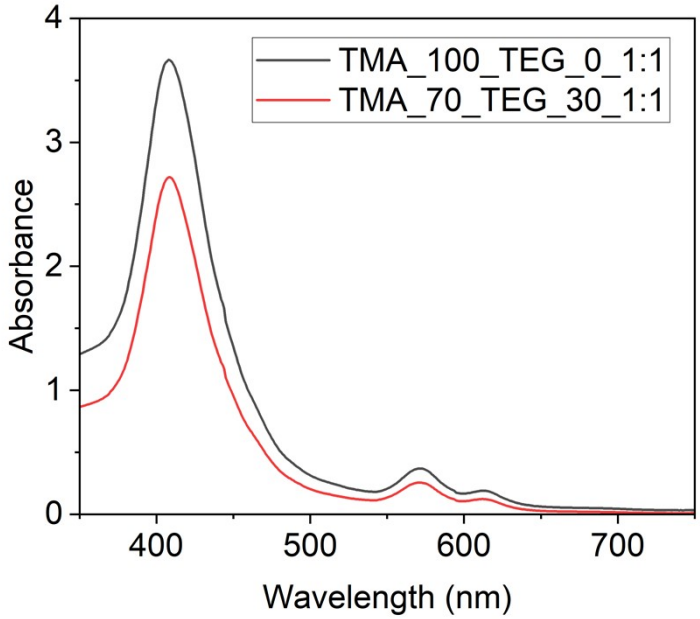

Supplementary Figure S6: UV/Vis spectra of TMA_100_TEG_0_1:1 and TMA_70_TEG_30_1:1 show differences in encapsulation between the two polyzymes based on FeTPP.

6.2. Transmission electron microscopy (TEM) and elemental mapping

Holy Carbon grids (400 mesh, copper) with ultrathin (3 nm) carbon film glow were discharged for 30 min at 20 mA. A 1 mg/mL solution in MilliQ water of the polyzymes TMA_70_TEG_30_1:1 and TMA_100_Teg_0_1:1 was cast on the grid and allowed to absorb for 1 min, respectively. Thereafter, the excess solution was removed, and 2-wt% Uranylacetate solution was applied for 15 sec. The respective grids were washed with 3 µL for three times. The bright field TEM was performed using a JEOL 2200FS EFTEM device operating at 200 kV. HAADF (High Angle Annular Dark Field) and EDS (Energy Dispersive X-Ray Spectrometer) acquisition was obtained using the same instrument equipped with an Oxford X-Max80 in the STEM (scanning transmission electron microscopy) mode (probe size = 1 nm) (**FigureS7-S9**).

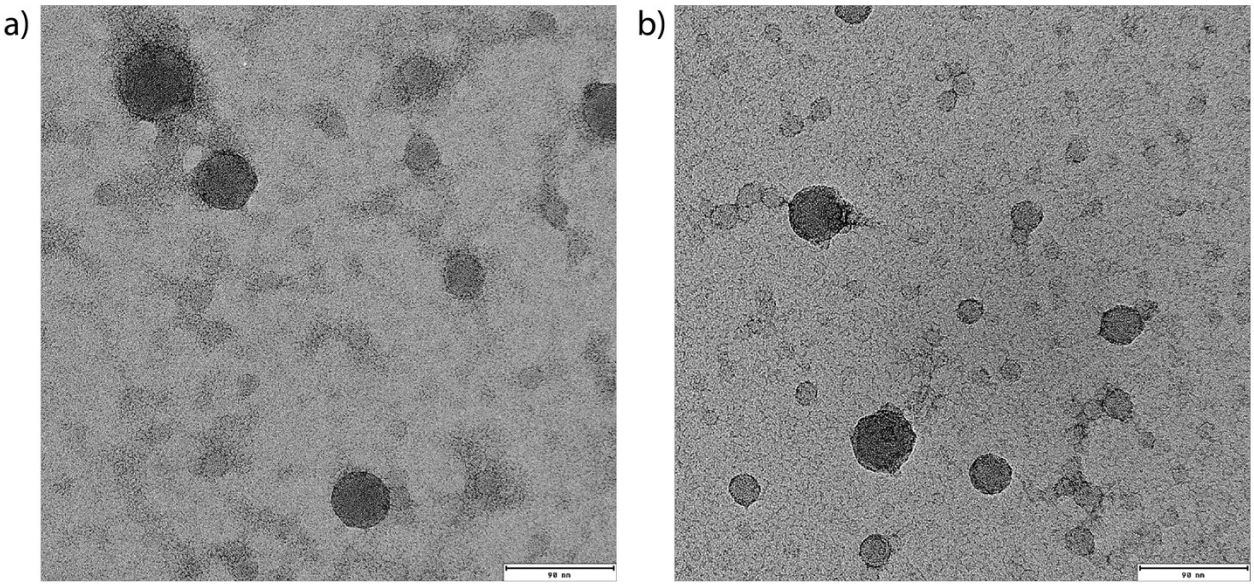

Supplementary Figure S7: TEM images of a) TMA_70_TEG_30_1:1 and b) TMA_100_TEG_0_1:1. Scale bar = 90 nm.

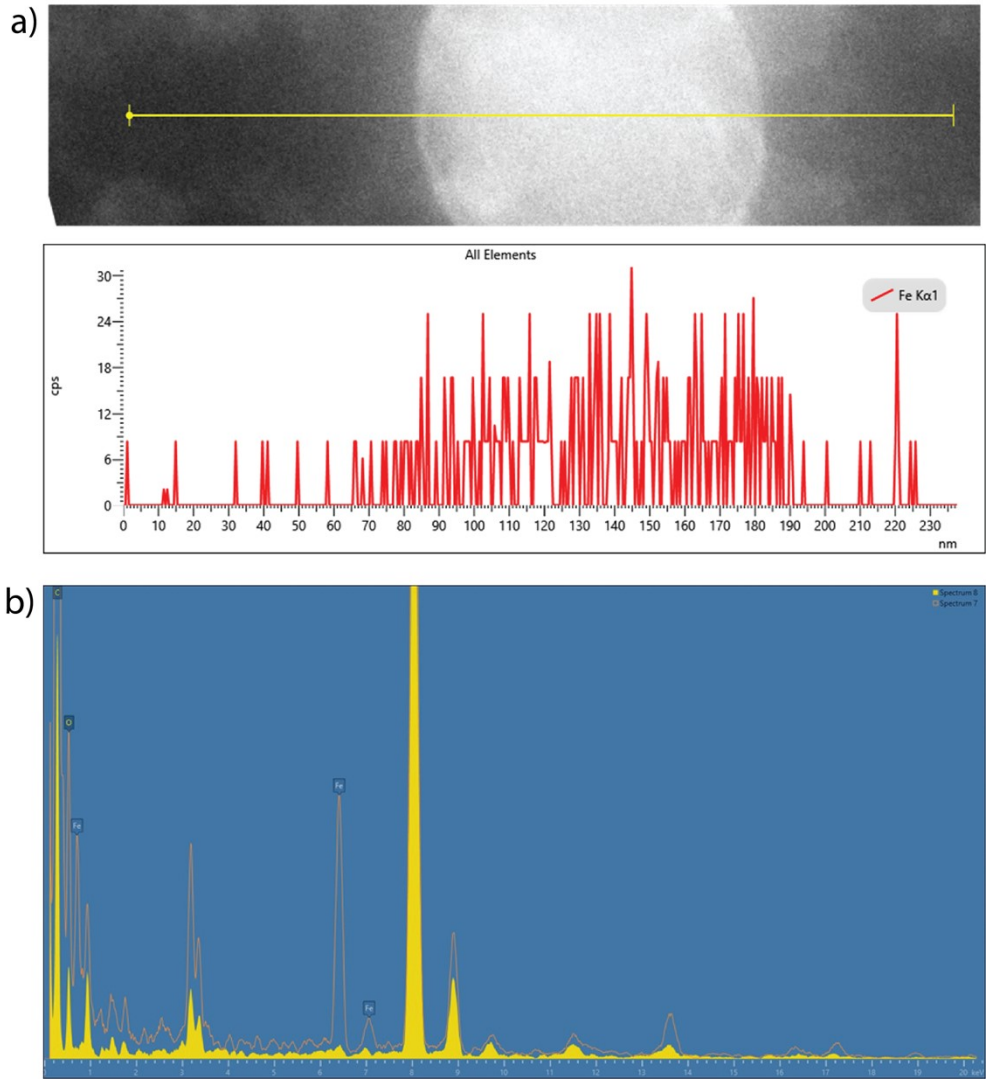

Supplementary Figure S8: a) EDS Line Scan reflecting Fe-content across one particle of **TMA_70_TEG_30_1:1**. b) EDS scan of **TMA_70_TEG_30_1:1** with the solid yellow representing the spectrum outside of the particle and the orange line representing the spectrum at the center of the particle. Additional non-marked peaks correspond to Uranium from the Uranylacetate stain and copper from the grid.

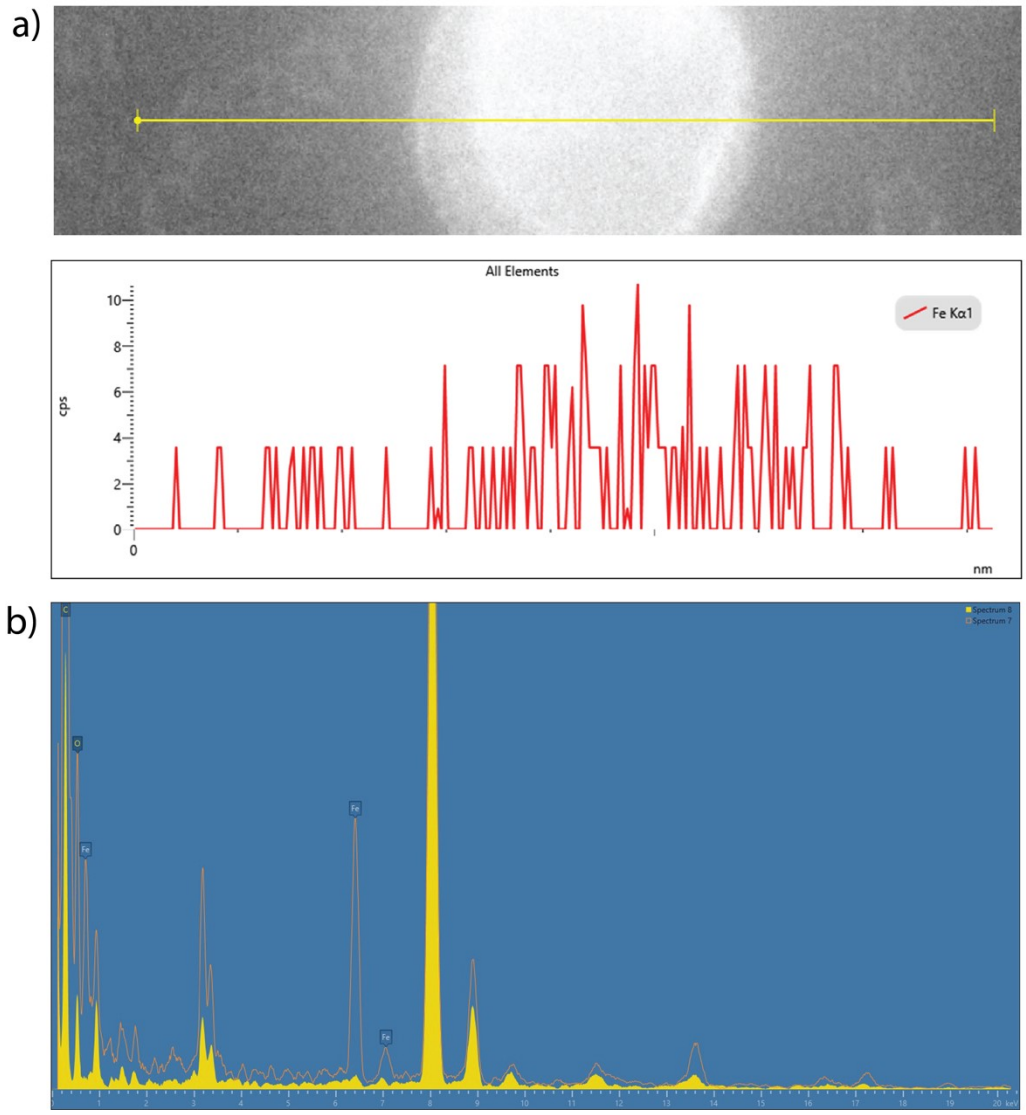

Supplementary Figure S9: a) EDS Line Scan reflecting Fe-content across one particle of **TMA_100_TEG_0_1:1**. b) EDS scan of **TMA_100_TEG_0_1:1** with the solid yellow representing the spectrum outside of the particle and the orange line representing the spectrum at the center of the particle. Additional non-marked peaks correspond to Uranium from the Uranylacetate stain and copper from the grid.

7. Nanozyme and FeTPP-mediated kinetics

In a black 96-well plate, the respective polyzyme, pro-rhodamine, and sodium ascorbate were combined to reach final concentrations of 200 nM, 10 µM, and 1 mM, respectively. The catalytic performance was monitored by measuring the fluorescence of rhodamine (ex. 488 nm, em. 521 nm) at different temperatures (25/28/31/37 °C).

As a control experiment, kinetics were performed with free FeTPP. Due to the insolubility of FeTPP in PBS (Figure S3), we dissolved FeTPP at maximum concentration soluble in DMSO (0.25 mg/mL, 0.350 mM).

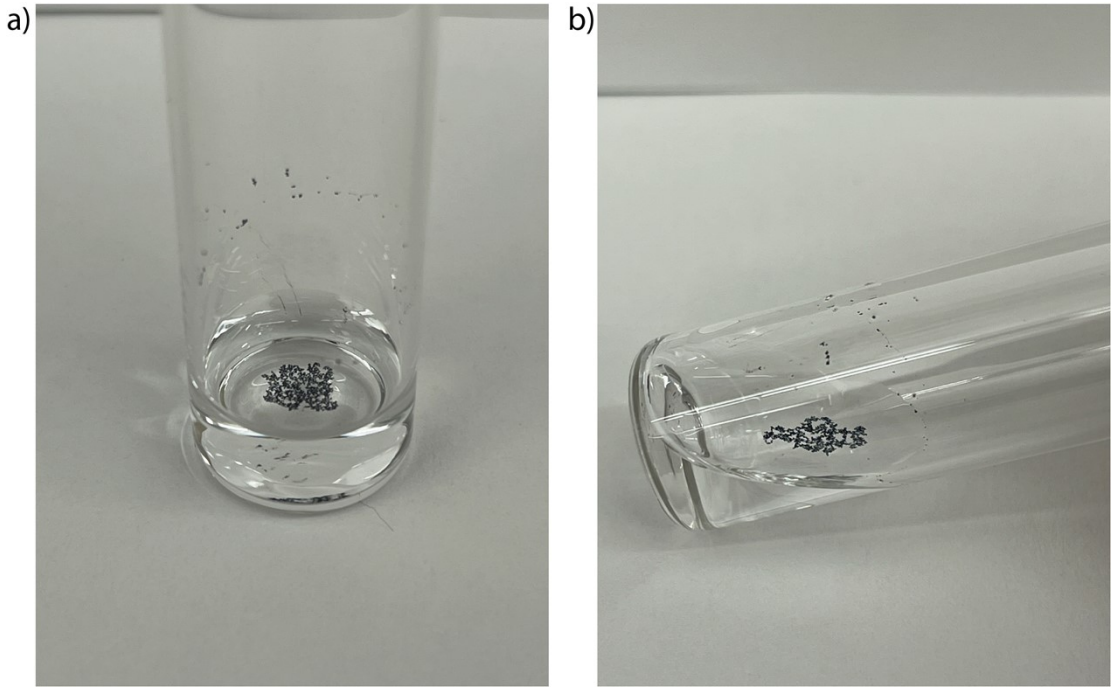

Supplementary Figure S10: Attempt to dissolve FeTPP (approx. 1 mg) in PBS.

A stock solution of FeTPP in PBS with 10% DMSO at 35 μM was prepared. For the kinetics experiment, a 5 mM stock solution of sodium ascorbate and a 25 μM stock solution of azide pro-Rhodamine were prepared. In a 96-well plate, 40 uL of the FeTPP stock solution, 40 uL of pro-Rhodamine stock solution, and 20 uL of sodium ascorbate stock solution were combined to reach final concentrations of 14 μM FeTPP, 10 μM pro-Rhodamine, and 1 mM sodium ascorbate in PBS (4% DMSO in well). Each experiment was performed in triplicate. FeTPP only and pro-Rhodamine only were used as controls. While FeTPP is catalytically active in water with 4% DMSO, low amounts of organic solvents can significantly impact cell viability.[4]

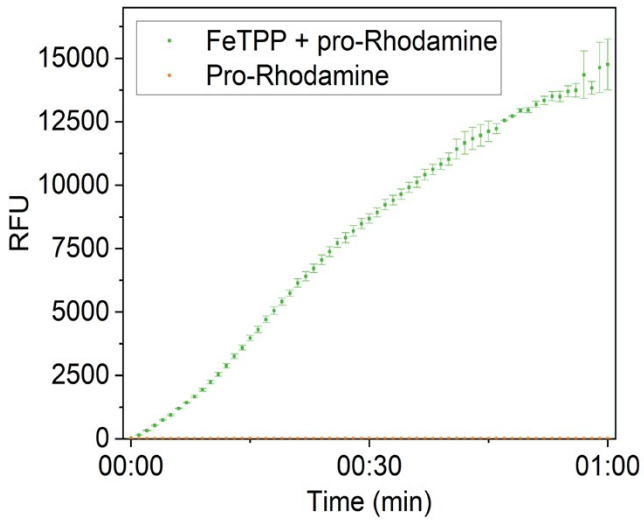

Supplementary Figure S11: Kinetics experiment with free FeTPP (14 μM FeTPP, 10 μM pro-Rhodamine, 1 mM sodium ascorbate).

8. Size of nanocatalyst determined by dynamic light scattering

Hydrodynamic diameter of the nanocatalyst (1 μM) was measured by dynamic light scattering (DLS) in saline phosphate buffer (PBS, pH=7.4), using a Malvern Zetasizer Nano ZS instrument. The measurement angle was 173° (backscatter). Data were analyzed by the "multiple narrow modes" (high resolution) based on non-negative-least-squares (NNLS).

9. Dynamic light scattering of nanocatalysts at different temperatures

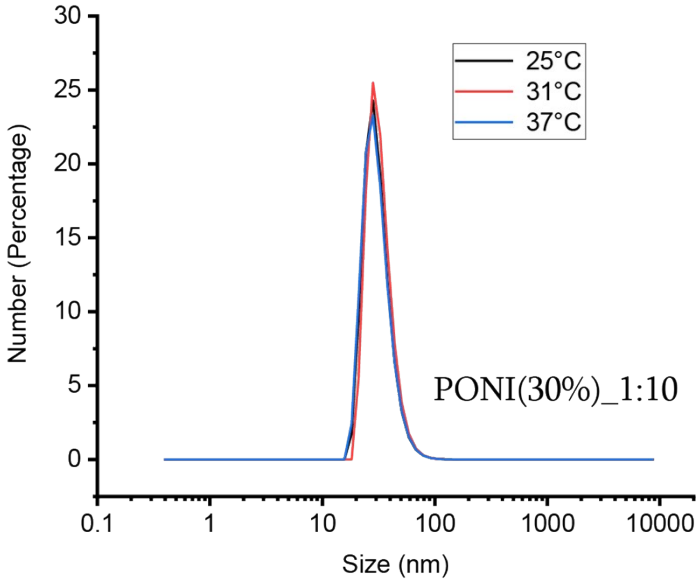

Supplementary Figure S12: DLS measurements demonstrated that the nanocatalyst did not experience any significant changes in size across the range of temperatures tested. This indicates that the thermo-responsive behavior of the nanocatalyst is not influenced by changes in particle aggregation or size.

10. Catalyst loading of nanocatalysts at different temperatures

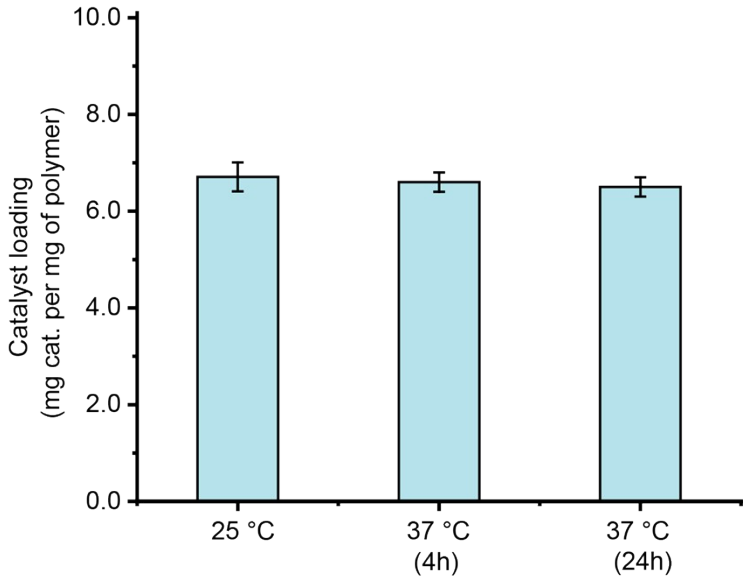

Supplementary Figure S13: Catalyst loading analysis of **TMA_70_TEG_30_1:10** revealed negligible changes in catalyst loading after incubation at 37 °C for 4 hours or 24 hours. This observation suggests

that there is minimal escape of FeTPP from the nanocatalyst structure during the incubation period, further supporting the confinement of FeTPP within the hydrophobic pocket.

11. Minimum biofilm inhibitory concentration of Cip and pro-Cip

E. coli bacteria (CD-2) were inoculated at 37 °C in TSB broth (2.5 mL/tube) until 0.5 McFarland standard. Then, 150 µL of this solution was seeded onto each well of a 96 well plate with pegged lid covered and cultured in a shaker at 50 rpm for 5 hours at 37 °C. Upon completion, the pegged lid was washed by transferring it onto a plate containing 200 µL PBS for 30 secs. The lid was then introduced onto another plate containing 200 µL of pro-Cip or Cip solution dissolved in M9 medium and incubated for 22 hours at 37 °C. MBICs were measured using optical density at 600 nm. M, molarity.

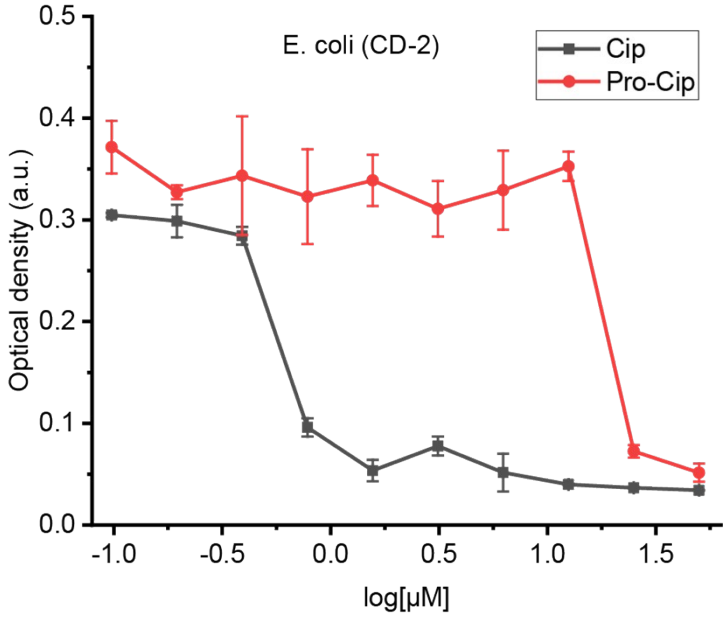

Supplementary Figure S14: minimum biofilm inhibitory concentration (MBIC) of Cip and pro-Cip toward *E. coli* (CD-2). The results showed that pro-Cip was less efficient to inhibit formation of CD-2 biofilm. We used established protocol with minor modification to test MBICs.[5]

12. Activation of pro-drug in bacterial biofilms

For the biofilm viability studies, 100 µL of *E. Coli* (CD-2) seeding solutions was added into each well of a 96 well-plate and incubated overnight at room temperature to grow the biofilms. The biofilms were then washed thrice with PBS and treated with the nanocatalyst (200 nM) and pro-Cip/Cip in M9 media. Bacterial biofilms were then incubated at 25 °C and 37 °C for 6 hrs. After this treatment, the biofilms were washed with PBS three times and their viability was determined using the Alamar Blue assay

according to the protocol established by the manufacturer. The activation of pro-Cip was further confirmed through a Ninhydrin Assay (**Figure S11**).

13. Validation of pro-Cip activation through Ninhydrin Assay

Various concentrations of pro-Cip were treated with 200 nM of **TMA_70_TEG_30_1:10** for 6 hours at 37 °C. The quantification of prodrug activation was subsequently carried out using a Ninhydrin assay, following a previously published protocol.[6,7]

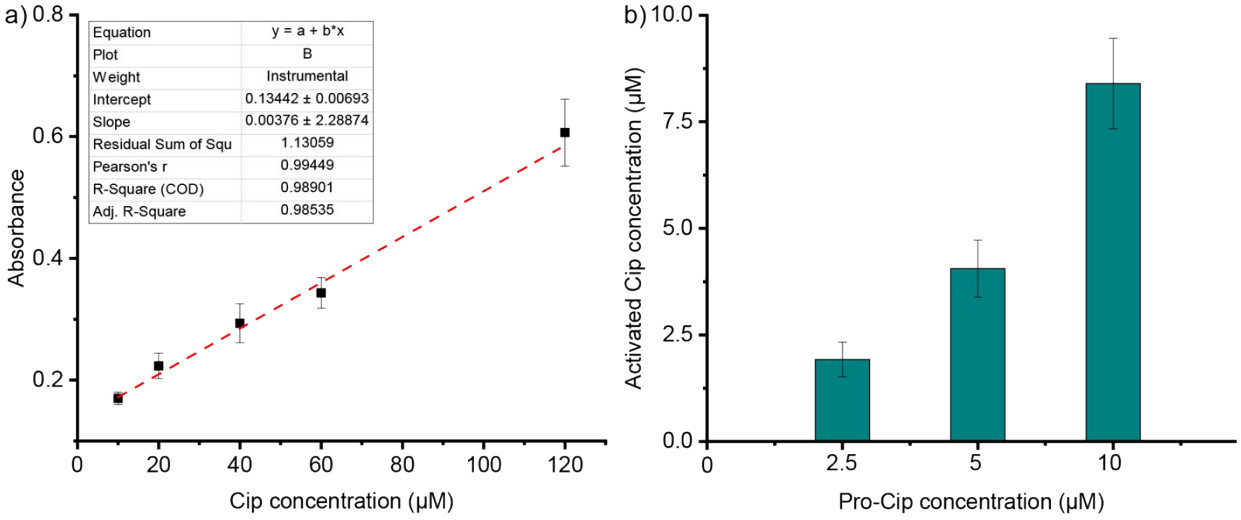

Supplementary Figure S15: a) Calibration curve of Cip using Ninhydrin assay. b) Equivalent ciprofloxacin concentration generated from pro-drug activation.

14. Synthesis of Pro-Rhodamine

The pro-Rhodamine was synthesized as described in reference 8.

15. Synthesis of pro-ciprofloxacin

The pro-ciprofloxacin was synthesized as described in reference 9.

1. A. Gupta, R. F. Landis, C.-H. Li, M. Schnurr, R. Das, Y.-W. Lee, M. Yazdani, Y. Liu, A. Kozlova and V. M. Rotello. *J. Am. Chem. Soc.* 2018, **140**, 12137–12143.

2. R. F. Landis, C.-H. Li, A. Gupta, Y.-W. Lee, M. Yazdani and V. M. Rotello. *J. Am. Chem. Soc.* 2018, **140**, 6176–6182.

3. J. B. Harland, A. B. Lalonde, D. J. Thomas, D. G. Castella, J. W. Kampf, M. Zeller, E. E. Alp, M. Y. Hu and J. Zhao, N. Lehnert. *Dalton Trans*. 2024, **53**, 13906-13924.

4. J. Galvao, B. Davis, M. Tilley, E. Normando, M. R. Duchen and M. F. Cordeiro. *FASEB* 2013, **28**, 1317-1330.

5. J. J. Harrison, C. A. Stremick, R. J. Turner, N. D. Allan, M. E. Olson and H. Ceri. *Nat. Protoc*. 2010, **5**, 1236–1254.

6. J. Hardie, J. M. Makabenta, A. Gupta, R. Huang, R. Cao-Milán, R. Goswami, X. Zhang, P. Abdulpurkar, M. E. Farkas and V. M. Rotello. *Mater. Horiz.* 2022, **9**, 1489–1494.

7. R. Cao-Milán, S. Gopalakrishnan, L.D. He, R. Huang, L.-S. Wang, L. Castellanos, D. C. Luther, R. F. Landis, J. M. V. Makabenta, C.-H. Li, X. Zhang, F. Scaletti, R. W. Vachet and V. M. Rotello. *Chem* 2020, **6**, 1113–1124.

8. P. K. Sasmal, S. Carregal-Romero, A. A. Han, C. N. Streu, Z. Lin, K. Namikawa, S. L. Elliott, R. W. Köster, W. J. Parak and E. Meggers. *ChemBioChem* 2012, **13**, 1116–1120.

9. R. Huang, C.-H. Li, R. Cao-Milán, L. D. He, J. M. Makabenta, X. Zhang, E. Yu and V. M. Rotello. *J. Am. Chem. Soc.* 2020, **142**, 10723–10729.